Surfaces and Interfaces 38 (2023) 102871

Contents lists available at ScienceDirect

Surfaces and Interfaces

journal homepage: www.sciencedirect.com/journal/surfaces-and-interfaces

Is carrier mobility a limiting factor for charge transfer in TiO_2/Si devices? A study by transient reflectance spectroscopy ☆

Ramsha Khan [a,*], Hannu P. Pasanen [a], Harri Ali-Löytty [b], Hussein M. Ayedh [c], Jesse Saari [b], Ville Vähänissi [c], Mika Valden [b], Hele Savin [c], Nikolai V. Tkachenko [a,*]

[a] Photonic Compounds and Nanomaterials Group, Faculty of Engineering and Natural Sciences, Tampere University, Tampere, 33700, Finland
[b] Surface Science Group, Faculty of Engineering and Natural Sciences, Tampere University, Tampere, 33014, Finland
[c] Department of Electronics and Nanoengineering, Aalto University, Tietotie 3, Espoo, 02150, Finland

ARTICLE INFO

Keywords:
Transient reflectance spectroscopy
Charge transfer
Titanium dioxide
Photoelectrochemistry
Atomic layer deposition

ABSTRACT

TiO_2 coatings are often deposited over silicon-based devices for surface passivation and corrosion protection. However, the charge transfer (CT) across the TiO_2/Si interface is critical as it may instigate potential losses and recombination of charge carriers in optoelectronic devices. Therefore, to investigate the CT across the TiO_2/Si interface, transient reflectance (TR) spectroscopy was employed as a contact-free method to evaluate the impact of interfacial SiO_x, heat-treatments, and other phenomena on the CT. Thin-film interference model was adapted to separate signals for Si and TiO_2 and to estimate the number of transferred carriers. Charge transfer velocity was found to be 5.2×10^4 cm s^{-1} for TiO_2 heat-treated at 300 °C, and even faster for amorphous TiO_2 if the interfacial SiO_x layer was removed using HF before TiO_2 deposition. However, the interface is easily oversaturated because of slow carrier diffusion in TiO_2 away from the TiO_2/Si interface. This inhibits CT, which could become an issue for heavily concentrated solar devices. Also, increasing the heat-treatment temperature from 300 °C to 550 °C has only little impact on the CT time but leads to reduced carrier lifetime of <3 ns in TiO_2 due to back recombination via the interfacial SiO_x, which is detrimental to TiO_2/Si device performance.

1. Introduction

Charge transfer (CT) processes within photoelectrodes are important factors for determining the proper functioning of photocatalytic devices [1]. In the case of photoelectrochemical (PEC) reactions, the photoelectrodes should be resistant to corrosion. Silicon is a light absorbing semiconductor which is extensively employed in various highly efficient and inexpensive devices since it is abundant in nature, and technologically well established. More recently, Si-based photoelectrodes are considered as potential alternatives for PEC devices [2,3]. However, the chemical instability of Si, in particular under alkaline conditions, prevents the use of Si photoelectrodes without a protection layer [4–6]. In acids, SiO_2 forms on Si that passivates the surface, and thus limits the CT process [7].

To overcome the stability problem, one approach is to deposit a protection layer on the Si photoelectrode [3,8–11]. Depositing metal oxide thin films can protect the surfaces of photoelectrodes from corrosion and if properly optimized, without compromising their catalytic activity [7,12]. TiO_2 has been employed widely since it is cost-effective, and photo- and chemically stable. So far, TiO_2 thin films grown by atomic layer deposition (ALD) have been exploited extensively to apply them as stable, conformal, and pinhole-free protective coatings on semiconductors for PEC applications [13–17]. Deposition of TiO_2 coatings by ALD is quite beneficial since it controls the layer growth on atomic level and can provide thin films with high quality [18–20]. ALD TiO_2 thin films are often amorphous containing various defects, such as Ti^{3+} intra-band gap defects close to the Fermi-edge which are responsible for exceptional charge transfer properties [19,21,22]. However, post-deposition heat-treatment in air at high temperatures (>300 °C) removes these defect states in the band gap and henceforth, improves the crystallinity of the thin films [23]. Also using ALD, TiO_2 coatings can be fabricated on Si without inducing the growth of any interfacial Si oxide that could be detrimental to the charge transfer [24].

Understanding the charge transfer mechanism and recombination dynamics is important for improving the efficiency of TiO_2/Si based

☆ This document is the results of the research project funded by Academy of Finland.
* Corresponding authors.
E-mail addresses: ramsha.khan@tuni.fi (R. Khan), nikolai.tkachenko@tuni.fi (N.V. Tkachenko).
URL: https://www.tuni.fi/en/nikolai-tkachenko (N.V. Tkachenko).

https://doi.org/10.1016/j.surfin.2023.102871
Received 18 November 2022; Received in revised form 15 March 2023; Accepted 8 April 2023
Available online 14 April 2023

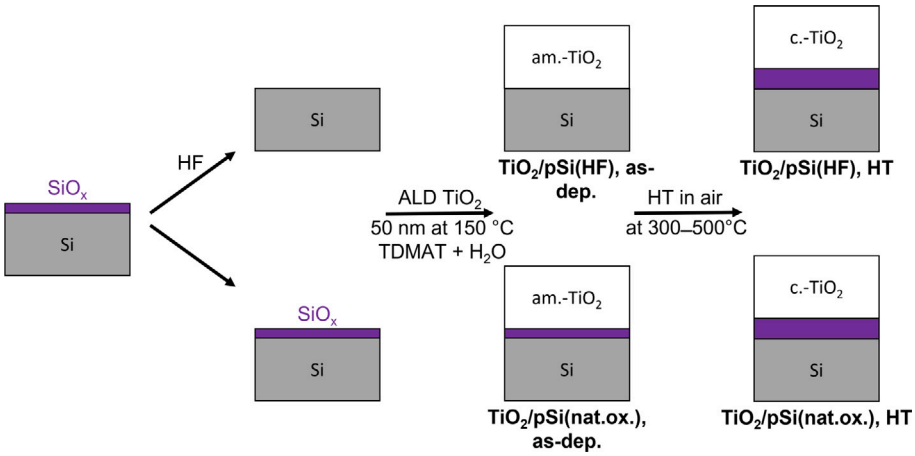

Fig. 1. Schematic of TiO_2 deposition by ALD with pre-deposition HF treatment and post-deposition heat-treatments at 300–550 °C.

PEC devices. Further advancement in the performance of these photoelectrodes is only possible from a deeper understanding of the limitations of the charge transfer from Si photoabsorber via TiO_2 protective coating to the catalytic reaction centres [25,26].

One of the main concerns for steady charge transfer is the interface between silicon and TiO_2 [24,27]. Interfacial Si oxide may form during processing of photoelectrodes and resist the charge transfer or induce recombination of charge carriers [28] which can cause failure of PEC devices. Also, in TiO_2 coatings, there are a lot of grain boundaries, and defects or trap states where the photocarriers can recombine [29,30]. Furthermore, the carrier mobility and diffusion length are very limited in TiO_2 [31] and in case of TiO_2/Si photocathodes, it should be taken into account that TiO_2 has n-type semiconductor electrical characteristics due to oxygen vacancies, with its conduction band almost aligned with the silicon [32] which affects the CT across the interface.

Currently in n-type solar cells, TiO_2 coating on Si is optimized to be used as electron selective contact resulting in high solar cell efficiencies [33,34]. The CT in solar cells is characterized indirectly by measuring the electron transport, i.e., the current via contact resistance measurement. However, PEC applications differ greatly from solar cells as the latter require only a thin TiO_2 layer to maximize the current transport whereas PEC typically requires a thicker, pinhole-free layer to provide resistance to corrosion. Moreover, when it comes to the top contact for TiO_2, which is electrolyte for PEC photoelectrodes and metal for solar cells, contact resistance measurements become less compatible with PEC photoelectrodes than contact-free optical methods.

To directly investigate CT from Si to TiO_2, we have devised a new method to study and understand the charge transfer across the TiO_2/Si interfaces using ultrafast time-resolved reflectance (TR). To the best of our knowledge, there is no prior analysis of electron transfer from Si to TiO_2 using ultrafast time-resolved techniques. The samples were prepared by atomic layer deposition (ALD) and we focus on the effects of post-deposition TiO_2heat-treatment temperatures and interfacial SiO_x on the CT properties by depositing TiO_2 on both native oxide and HF pre-treated oxide free p-type Si (pSi). We then separate TR signals of TiO_2 and Si by varying the excitation wavelength to selectively excite either one of the materials, and through thin-film interference (TFI) modelling [35] and then provide detailed information on the charge transfer velocity, back recombination, and any potential bottlenecks the carriers may encounter. Finally, for providing some additional support to our TR results, we probe in specific samples the band bending/the surface barrier (V_{sb}) on silicon surface induced by the TiO_2 thin films using corona oxide characterization of semiconductor (COCOS) technique [36]. We also characterize the samples with microwave photoconductive decay (μ-PCD) measurements to test how well the surface is passivated for the minority carriers.

2. Experimental

2.1. Sample preparation

Atomic layer deposition (ALD) of TiO_2 was carried out using a Picosun Sunale ALD R200 Advanced reactor. Tetrakis(dimethylamido) titanium(IV) ($Ti(N(CH_3)_2)_4$), TDMAT, electronic grade 99.999+ %, (Sigma-Aldrich, Inc.), ultrapure Milli-Q water, and Ar (99.9999%, Oy AGA Ab, Finland) were used as the Ti precursor, O precursor, and carrier/purge/venting gas, respectively. TiO_2 films (1060 ALD cycles, 50 nm) were grown at 150 °C using previously reported process [22, 37–39]. The TiO_2 film thickness was optimized to minimize the effect on interference pattern on transient absorption spectra. B-doped (resistivity: <0.005 Ω cm) p-type Si(100) (pSi) wafers from SIEGERT WAFER GmbH (Germany) were used for charge transfer studies using optical TR method.

Two sets of samples were fabricated. For the first set, ALD TiO_2 films were grown on Si with native Si oxide film at the surface. For the second set, the native Si oxide film was removed by hydrofluoric acid (HF) treatment prior to the ALD deposition [24]. The schematic of sample preparation is shown in Fig. 1. Post deposition heat treatment (HT) was applied at 300 °C (HT or 300HT), 400 °C (400HT), and 550 °C (550HT) for 1 h in ambient air to convert amorphous TiO_2 (am.-TiO_2) into anatase TiO_2 (c.-TiO_2) [22] and to induce formation of interfacial Si oxide. Saari et al. have showed that, despite the initial removal of native SiO_x by HF, the thickness of interfacial SiO_x increases linearly with the HT temperature from 0.7 nm (200 °C) to 3.2 nm (550 °C) [24].

3. Methods

3.1. Steady state spectroscopy

The steady state reflectance spectra of the samples were recorded using Shimadzu UV-3600 UV–Vis-NIR spectrophotometer in reflectance mode. A 'Specular Reflectance Attachment for 5° Incidence Angle' accessory was used with the spectrophotometer setup. Aluminium coated mirrors were used for reference. The measurements were taken from 300 to 1200 nm.

3.2. Transient absorption spectroscopy

For studying the optical properties of samples, the ultra-fast time-resolved pump-probe spectroscopy was used in reflectance mode. The fundamental laser pulses were generated via Ti:Sapphire laser (Libra F, Coherent Inc., 800 nm, approx. 100 fs pulse width, repetition rate

1 kHz). 90% of the fundamental beam was directed onto optical parametric amplifier (Topas C, Light conversion Ltd.) to produce the desired excitation wavelength (320 and 500 nm in our case), approximately 1 mm diameter at the sample, attenuated up to 456 μ J cm^{-2}. Different excitation wavelengths were used to excite the samples at different penetration depths and to induce excitation in the Si substrate only (with 500 nm excitation). 10% of the fundamental laser was delivered to motorized stage (delay line) and then to a 2 mm cuvette with water to generate continuum white light for probe pulses. The probe light was split into the reference and signal beams. The absorbance change was measured in chopper mode which is synchronized with fundamental laser pulses. The spectra were averaged over 2000 excited pulses for each delay time.

3.3. TiO_2 induced surface barrier and silicon minority carrier lifetime characterization

The band bending/surface barrier (V_{sb}) at the silicon sample surface induced by the TiO_2 thin films was measured in specific samples (n-type substrates, with and without HF dip, 300 °C HT samples) using COCOS method, which is described in Reference [36]. (Note that the degenerately doped p-type substrates had too high doping concentration and resulting Auger recombination rate limiting the bulk Si lifetime has very low values (<1 μs) [40], making the samples unsuitable for COCOS measurements.) To study the quality of the electrical surface passivation provided by the TiO_2 thin films on silicon, the effective minority carrier lifetime in the samples was measured by μ-PCD. A full-sample μ-PCD lifetime scan was performed with a 904 nm pulsed laser using a raster size of 1 mm and by averaging of 16 measured values per point. In addition to double-side TiO_2-coated samples, the measurement was done also for reference samples without any TiO_2 thin film on either surface.

4. Modelling theory

4.1. Steady state reflectance modelling

The steady state reflectance of the samples was measured in the range of 300–1200 nm. To determine the TiO_2 coating thickness, the reflectance of the samples was modelled and fitted to the measured spectra. It was assumed that either the HF treatment [24] or the post-deposition annealing [38] had only a little effect on the TiO_2 film thickness. The modelled steady state reflectance spectra are obtained by using transfer-matrix based thin-film interference model, TFI, which takes into account thickness, refractive index, and absorption of TiO_2 and Si [41]. In short, transfer-matrix calculates the reflectance at each interface and absorption in each layer and then it sums the resulting total interference and reflectance of the sample. The refractive index and absorption coefficient data of Si and TiO_2 were acquired from Aspnes et al. [42] and DeVore et al. [43], respectively, but the refractive index of TiO_2 was increased by 5% to better reproduce the measured steady-state reflectance. Additionally, the Si substrates were not polished from the back side which removed the back reflectance also in the NIR region. Therefore, it acts as a thick absorbing wafer that has no reflection from the back side of the wafer, and hence it was treated as infinitely thick in the model as shown below. However, interfacial SiO_x layer has not been added to the model because it was too thin (< 3 nm) to have significant effect on the simulations, and addition of SiO_x to the model could be compensated by simply reducing the thickness of the TiO_2 layer.

Monitoring light → | TiO_2 thin layer | Si thick layer

4.2. Transient reflectance modelling

Transient photoinduced reflectance was modelled using the same transfer-matrix based TFI model. Information on the model can be found in our previous publication [35]. After modelling the steady-state reflectance spectra, we also modelled the change in reflectance after the excitation which is caused by the photogenerated carriers as they produce a change in the refractive index, Δn, and absorption coefficient, $\Delta \alpha$, of the sample. The TR response in optical density (OD) units is then calculated by comparing these reflectance spectra. Excited state carrier distribution is taken into account by splitting the modelled film into multiple layers. For instance, 57 nm TiO_2 layer was split into 57 separate layers, each with Δn and $\Delta \alpha$ multiplied by the relative carrier concentration in that layer. Similarly, pSi was split into 3000 layers, each 5 nm thick. The Δn and $\Delta \alpha$ for TiO_2 were based on data for TiO_2 on glass from our previous publication [22] with minor adjustments to improve the simulated TR spectra for both the 320 nm excitation signal and the CT induced signal. Both the 320 nm excitation and CT signal by 500 nm excitation were modelled with the same Δn and $\Delta \alpha$ shown in Figure S1.

Furthermore, only Δn was estimated from bare pSi substrate since TR response of bare pSi is not sensitive to changes in absorption due to the lack of thin film interference. The sensitivity to $\Delta \alpha$ increases when TiO_2 is deposited on Si, and a small $\Delta \alpha$ was introduced to adjust the modelled TR response of TiO_2/pSi(HF), 300HT sample (see Section Δn and $\Delta \alpha$ fit: linear approximation in SI). The sensitivity of Δn and $\Delta \alpha$ to TR simulations on pSi and TiO_2/Si samples are shown in Figure S2.

The bare pSi and TiO_2/pSi(HF), 300HT samples were modelled using the TFI model. TiO_2/pSi(nat. ox.), 300HT sample had very similar spectra so it was not modelled separately. Furthermore, the as-dep. TiO_2 samples were not modelled because their optical properties and Δn and $\Delta \alpha$ values are different and less clear than those of the heat-treated samples, but the same approach can be applied.

4.3. Diffusion model

To account for the diffusion of carriers in the heat-treated TiO_2/pSi samples, TR measurements were done by varying the excitation wavelengths. The initial carrier distribution is given by Eq. (1).

$$N(x,0) = N_0 \times \exp(-\alpha x) \tag{1}$$

where N_0 is the initial surface carrier density, such that $N_0 = \alpha(1-R)J_0$, where J_0 is the pump fluence and R is the reflectance at the excitation wavelength. Carrier dynamics is then modelled with 1-D diffusion as shown in Eq. (2) with boundary conditions as shown in Eqs. (3) and (4).

$$\frac{\partial N(x,t)}{\partial t} = D\frac{\partial^2 N(x,t)}{\partial x^2} \tag{2}$$

where $N(x,t)$ is the carrier density at depth (x) and time (t), and D is the diffusion coefficient.

$$\left.\frac{\partial N(x,t)}{\partial t}\right|_{x=0} = \frac{V_{CT}}{D}N(0,t) \tag{3}$$

and

$$\left.\frac{\partial N(x,t)}{\partial t}\right|_{x=L} = 0 \tag{4}$$

where L is the modelling depth of Si substrate and V_{CT} is the charge transfer velocity. Carriers in Si were modelled in a Si film with thickness down to 15 μm on the top of a 525 μm thick Si wafer, in other words, the Si surface is treated as a film purely for modelling purposes. The modelled Si layer of 15 μm is thicker than the optical penetration depth plus carrier diffusion length in Si in 5 ns time scale. At 500 nm, the penetration depth for Si is roughly 1 μm which is calculated from the absorption coefficient, α. At 500 nm, the α for Si is 1.1×10^4 cm^{-1} [44]. For fitting the V_{CT}, the number of carriers in the diffusion simulation were summed at each delay time and all carrier losses were assigned as charge transfer to TiO_2 via interfacial SiO_x (simulation had no other recombination and no loss of carriers at the back side of Si).

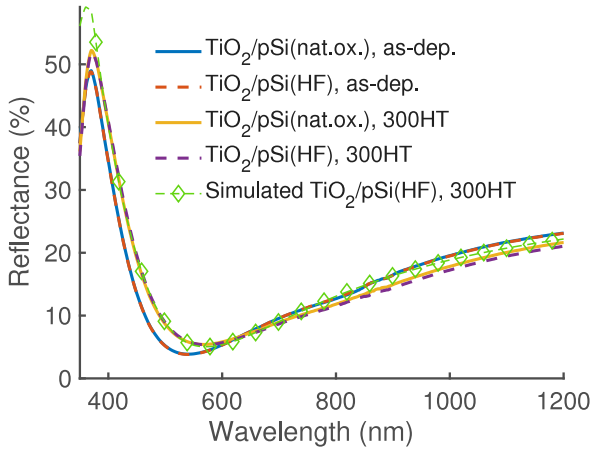

Fig. 2. Measured steady state reflectance of the as-deposited and 300HT samples. TiO_2/pSi(HF), 300HT sample was simulated to determine the thickness of TiO_2 layer deposited on pSi which is estimated to be 57 nm.

5. Results and discussion

5.1. Steady state reflectance

The measured steady state reflectance spectra of TiO_2/pSi samples were obtained in the range 300–1200 nm and are shown in Fig. 2. The substrate pre-treatments had little effect on the reflectance spectra. However, the post-deposition heat-treatment induced a substantial change to the reflectance due to the amorphous to anatase TiO_2 phase transition [22]. The nominal thickness of ALD TiO_2 thin film was 50 nm. Fig. 2 also shows the modelling of TiO_2/pSi(HF), 300HT sample. However, the modelled spectrum was fitted to the measured reflectance spectrum and resulting thickness of TiO_2 coating was found to be 57 nm. The model is described in Section 4.1. The interfacial SiO_x layer did not impact the simulations as long as thickness of TiO_2+ SiO_x equalled 57 nm for steady state, as the addition of small amount (<3 nm) interfacial SiO_x mainly shifts the spectra in the same manner as additional TiO_2 thickness.

5.2. Transient reflectance measurements

To see whether the charge transfer takes place from pSi to TiO_2, the TR spectra of samples grown on HF-treated pSi were measured. The samples were first excited at 500 nm with energy density of 200 μ J cm^{-2} since the heat-treated TiO_2 does not absorb in the visible region.

The measured TR spectra of bare pSi substrate and TiO_2/pSi(HF), 300HT samples are presented in Fig. 3a and 3b, respectively. For bare pSi, the TR spectra is only positive but with TiO_2 coating, it shows that at longer delay times, >500 ps, the negative signal recovers partially and shifts its maximum to the blue region and then positive ΔR grows in the red region. To evaluate the TR spectra that stems from pSi alone before any charge transfer, the transfer matrix based TFI model is employed to simulate the signal generated by carriers in pSi (see the modelling Section), which is then compared to the measured TR spectra at 1 ps. This was done to confirm that the TR spectrum at this delay time is coming from (free) carriers in silicon. The simulated TR spectrum for photoexcited carriers in Si matches with the measured spectra as shown by green line in Fig. 3b, and therefore the rise of the positive signal in the red region (600–750 nm) after 500 ps is indicative of charge transfer from pSi to TiO_2 via interfacial SiO_x.

Fig. 3c shows the measured TiO_2/pSi(HF), 300HT decay signal (black line) at 600 nm probe wavelength. It is compared to the normalized decay of bare pSi TR response (orange curve) under similar excitation conditions. The decays clearly deviate from each other after 100 ps, which we attribute to charge transfer from Si to TiO_2 via interfacial SiO_x. The fitting for decay signals of the pSi substrate was done by one-dimensional diffusion of charge carriers with diffusion constant of 15 cm^2 s^{-1} and the decays are shown in Figure S6 under various excitation wavelengths. No significant recombination was detected in any of the bare pSi (with native oxide) sample measurements regardless of the pump excitation wavelength.

5.3. Carrier distributions in TiO_2 and their respective signals

In order to analyse the CT in greater detail, we proceeded to extract the TR spectra of TiO_2 rising from the CT by removing the presumably remaining TR signal from pSi. The decay fit of pSi substrate signal (normalized to match the measured TiO_2/pSi(HF), 300HT at 10 ps delay time) was subtracted from the TR spectra of TiO_2/pSi(HF), 300HT, and the results are shown in Fig. 4a and 4b. Fig. 4a shows the extracted TiO_2 TR spectra at different delay times, and Fig. 4b shows the TiO_2 signal rise as a function of time at various wavelengths. The characteristic time when half of the TiO_2 signal appears for TiO_2/pSi(HF), 300HT sample is roughly 370 ps.

Next let us compare this extracted TiO_2 CT signal to the direct excitation of TiO_2 by using 320 nm pump. The TR spectrum of TiO_2 after 320 nm excitation and 1 ps delay time is given in Fig. 5a, whereas the rest of the decay spectra for this measurement are shown in Figure S3. The spectrum shows both positive and negative signals in the wavelength ranges 400–600 nm and 600–750 nm, respectively, which are due to thin film interference pattern [37]. However, the CT induced TiO_2 spectrum that was discovered in the previous section with excitation at 500 nm is almost the exact opposite of the TiO_2 spectra when excited directly at 320 nm. Therefore, we simulated both signals, CT after 500 nm excitation and the 320 nm direct excitation, by applying the carrier distributions shown in Fig. 5b. For the carrier distribution after CT, an exponential distribution is employed to simplify the modelling. The steepness of the exponent (in other words, width of the distribution) was used as a fitting variable until the simulated CT spectrum matched the extracted CT spectrum as shown in Fig. 5a. Both of the simulated spectra are quite in tone with their respective measured and extracted spectra, which confirms that CT is indeed happening through the interfacial SiO_x to the TiO_2. However, the simulation also shows that the transferred carriers are staying very near the TiO_2/pSi interface.

Modelling the TR spectra of TiO_2 under both circumstances, when excited from the front by 320 nm pump or when accepting electrons from pSi with 500 nm excitation allowed us to accurately estimate the number of carriers that had been transferred from pSi to TiO_2 at each delay time. The TR results by 320 nm excitation allowed us to estimate that how large Δn and $\Delta \alpha$ is produced per excited carrier, and by using the same model for the charge transfer (expect flipping the carrier distribution to the other side of the film as in Fig. 5b) we could fit the Δn and $\Delta \alpha$ in the case of charge transfer and calculate them back into the number of transferred carriers. The fit for the 320 nm excitation (8×10^{13} photons/cm^2 or photoinduced electrons/cm^2) gave us a baseline of Δn and $\Delta \alpha$ (shown in Figure S2). In turn, the extracted CT spectra at 1 ns in Fig. 4a (same as in 5a) corresponded to a multiplier of 0.42. This value told us how many carriers had been transferred:

$$0.42 \times 8 \times 10^{13} \text{ electrons/cm}^2 = 3.33 \times 10^{13} \text{ electrons cm}^{-2} \quad (5)$$

This was then compared to the total number of photogenerated carriers by the 500 nm excitation with density of 200 μ J cm^{-2}, which produced 5.14×10^{13} electrons/cm^2, and thus the percentage of transferred carriers was 6.5% during 1 ns. Majority of the carriers escape to the bulk pSi, but that is expected since the pump penetration depth is approx. 1 μm. This estimate applies only to the measurement carried out on TiO_2/pSi(HF), 300HT sample with 200 μ J cm^{-2} excitation density (at 500 nm excitation), as the percentage of transferred carriers depends greatly on the excitation energy density, as shown in the next Section.

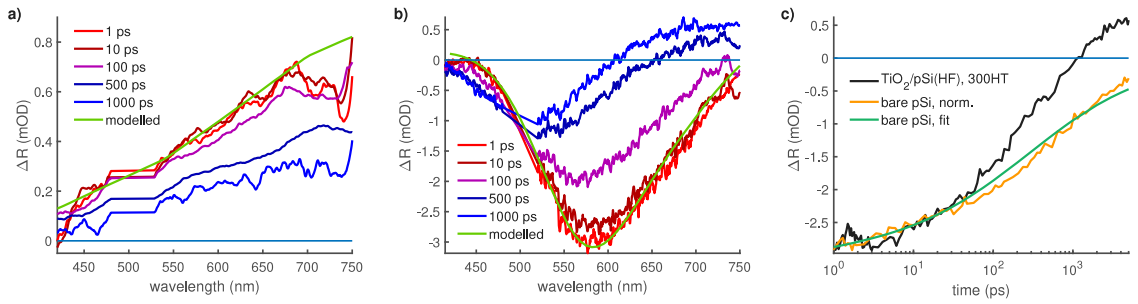

Fig. 3. Excitation of samples at 500 nm with 200 μ J cm^{-2} (a) TR spectra of bare pSi substrate at different delay times where signal at 1 ps was also reproduced using the TFI model (green line), (b) TR spectra of TiO_2/pSi(HF), 300HT sample at different delay times where signal at 1 ps was also reproduced using the TFI model (green line), (c) comparison of TiO_2/pSi(HF), 300HT signal decay (black) at 600 nm to measured (orange line) and fitted (green line) decays of pSi substrate normalized at 1 ps. (For interpretation of the references to colour in this figure legend, the reader is referred to the web version of this article.)

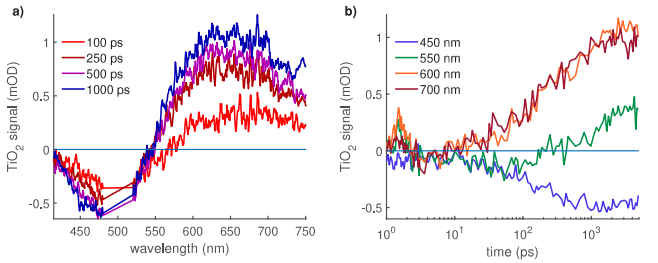

Fig. 4. Extracted TiO_2 signal after excitation of TiO_2/pSi(HF), 300HT at 500 nm with 200 μ J cm^{-2} where (a) shows the spectra over time and (b) the rise of the signal at different wavelengths as function of time.

Table 1
Percentage of charge carriers which transfer from pSi to TiO_2 at different energy densities in TiO_2/pSi(HF), 300HT sample within 1 ns and the corresponding charge transfer velocity.

Energy density, μ J cm^{-2}	Transferred charge carriers, %	Charge transfer velocity , 10^4 cm s^{-1}
24	24	5.2
80	11	1.96
144	7.2	1.22
200	6.5	1.07
456	4.3	0.70

5.4. Power dependence of CT from pSi to TiO_2

In previous sections, the clear shift in measured spectra verifies that the charge transfer is taking place from pSi to TiO_2, and by extracting the TiO_2 signal, the CT can be witnessed clearly. However, the charge transfer apparently stops at longer delay times, and in order to investigate this we performed the same measurements with excitation at 500 nm at various energy densities and thus, TiO_2 TR spectra were extracted using the same approach to analysis.

Fig. 6 shows the extracted TiO_2 signal as function of energy density from 24 to 456 μ J cm^{-2} (the original measured data is given in Figure S4). Fig. 6a shows how TiO_2 spectral maximum shifts from 700 to 600 nm, but the signal maximum increases by only 3 times when the excitation energy density is increased by close to 20 times. The rise of the TiO_2 signal at 700 nm probe is shown in Fig. 6b. Based on our earlier knowledge that the charge carriers remain near the interface, we presume that the low diffusion coefficient of electrons in TiO_2 prevents carriers from leaving the interface, leading to oversaturation of the interface and inhibition of further charge transfer. In other words, all possible carrier states in TiO_2 are occupied as the carriers in both pSi and TiO_2 are approaching the same energy levels.

The percentage of charges getting transferred from pSi to TiO_2 at different energy densities is tabulated in Table 1. The table also shows fitted V_{CT} over 1 ns for each measurement in Fig. 6b. However, due to eventual over-saturation of the TiO_2/Si interface, the initial V_{CT} is much faster in all measurements. The V_{CT} fit for the lowest pump fluence (24 μ J cm^{-2}) is shown in Fig. 6b, which shows that even with this low excitation power the charge transfer is still bottle-necked after 1 ns. The corresponding carrier distributions in Si at each delay time are shown in Figure S7. Nonetheless, this oversaturation induced limitation of CT should not be an issue for regular devices under unconcentrated solar illumination. For estimation, it requires approx. 1 μ s for electrons to reach to the surface of TiO_2, see SI Section 6. For a hypothetical concentrated solar cell device with 100% efficiency and 1000 sun illumination, energy output in 1 μ s is almost 136 μ J cm^{-2} (SI Equation S10). However, at excitation density of 24 μ J cm^{-2} the charge transfer efficiency is only 24% (see Table 1) meaning that the carrier oversaturation at the TiO_2-Si interface takes place at a few μ J cm^{-2} excitation density. Therefore, the 1000 times solar light concentration may result in the photo-carrier density more than 20 times higher than the saturation limit, thus, reducing the efficiency of the interfacial charge transfer to a few percent. Nonetheless, devices with lower concentration are unlikely to reach this performance limitation. Furthermore, the relaxation of the saturated interface is outside our measurement range of 5 ns, and we cannot say how many tens or hundreds of nanoseconds the interface remains saturated. However, highly concentrated solar devices [45,46] could thus run into this problem.

5.5. Effect of HF- and heat-treatment

To demonstrate the effect of HF treatment on pSi substrates, the samples were excited at 500 nm at both low (24 μ J cm^{-2}), and high (200 μ J cm^{-2}) pump fluence, shown in Fig. 7. At low power excitation, both samples deposited on nat.ox. pSi, regardless of heat-treatment, showed no TiO_2 signal, whereas samples deposited on HF-treated pSi both showed a TiO_2 signal of approx. 0.5 mOD. This elucidates that the removal of native SiO_x before ALD results in enhanced charge transfer for both as-dep. and HT samples. What is surprising is that the heat-treatment has been shown to induce the growth of equally thick interfacial SiO_x layer on both samples regardless of the HF pre-treatment [24]. Therefore, our results reveal that the interfacial Si oxide that grows at a Si oxide-free TiO_2/Si interface during the HT has more facile CT properties. That is why CT is sensitive to even subtle differences in the interfacial Si oxide. It is suggested that the interdiffusion between TiO_2 and growing interfacial SiO_x [47] is stronger when the interfacial Si oxide grows at an oxide-free Si compared to the native Si oxide, which can explain the observed difference. The surface barrier values obtained from the COCOS measurements using n-type doped Si substrates further support this. When the native oxide was removed with the HF dip prior to the TiO_2 deposition, the surface barrier height after HT at 300 °C decreased approximately with a factor of 2 (0.34 V vs. 0.14 V). The barrier height by COCOS using the degenerately doped

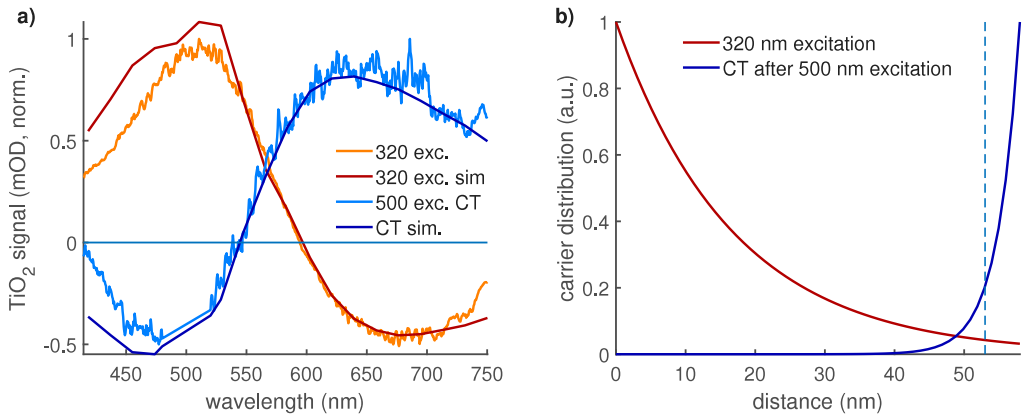

Fig. 5. Modelled TiO_2 signals for TiO_2/pSi(HF), 300HT sample with different carrier distributions compared to measured TiO_2 signals either due to 320 nm excitation (direct excitation) or charge transfer from pSi with 500 nm excitation. (a) Measured and simulated TR spectra of TiO_2 at 1 ps after 320 nm excitation (light orange and dark red lines, respectively), and extracted and modelled charge transfer signal of pSi at 1 ns (light and dark blue lines, respectively). (b) Normalized carrier distribution in TiO_2 after 1 ps with 320 nm excitation (red line), and fitted carrier distribution due to charge transfer from pSi to TiO_2 (blue) at 1 ns with 500 nm excitation and dashed light blue line is depicting 5 nm from the TiO_2/pSi interface, where most of the transferred carriers are staying. (For interpretation of the references to colour in this figure legend, the reader is referred to the web version of this article.)

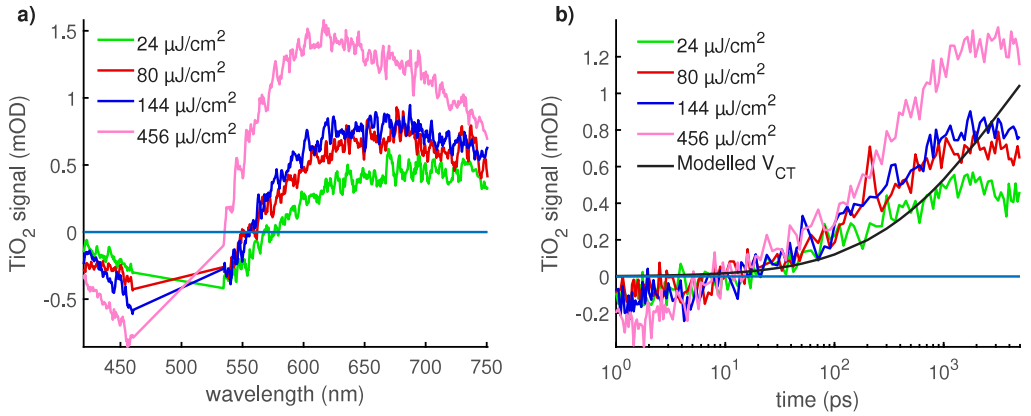

Fig. 6. (a) TR spectra extraction of TiO_2 charge transfer signal obtained at different power densities at 1 ns delay time, (b) Comparison of measured decay dynamics of TiO_2/pSi(HF), 300HT sample when excited at 500 nm with different power densities at 700 nm probe wavelength, and the black line is the modelled number of transferred carriers with V_{CT} of 5.2×10^4 cm s^{-1} corresponding to 24 μ J cm^{-2} and normalized to match it at 1 ns. The black line keeps rising after 1 ns because, in the model, there are still carriers at the Si side of the interface that can transfer to TiO_2 (see Figure S7). (For interpretation of the references to colour in this figure legend, the reader is referred to the web version of this article.)

p-type Si could not be measured due to high concentration of majority carriers in the substrate.

However, in the case of sample excitation at high power (200 μ J cm^{-2}), all the samples showed characteristic TiO_2 signal. The time where this characteristic appears halfway for all the samples is tabulated in Table 2. The samples without HF treatment manifest TiO_2 signal 5–10 times slower as shown in Fig. 7b. Also, the as-deposited samples, i.e., with amorphous TiO_2, do not appear to have difference in CT times when compared to the HT samples, i.e., with crystalline TiO_2. However, with HF treatment the as-dep. sample, the only sample without any interfacial SiO_x, had the fastest characteristic CT time suggesting detrimental role of interfacial SiO_x to the CT. However, the difference is not very large, implying that small amounts of interfacial SiO_x can be tolerated without major inhibition to CT.

The schematic of TiO_2/Si system is shown in Fig. 8. The heat-treatment at 300–550 °C induces crystallization of these TiO_2 films into anatase phase which in turn increases the lifetime of photoinduced carries within TiO_2 when it is excited at 320 nm [22] as shown in Figure S9. However, after 500 nm excitation and CT to TiO_2, even the carriers in amorphous TiO_2 have very long lifetime, and the back recombination with holes in Si takes more than 5 ns, and this also applies to the 300HT samples. Despite the initial removal of native SiO_x by HF, the thickness of interfacial SiO_x that form during the heat-treatments increases linearly with the HT temperature from 0.7 nm (200 °C) to 3.2 nm (550 °C) [24]. Additional samples were prepared with heat-treatments at 400 °C and 550 °C to observe how increasing the amount of interfacial SiO_x affects the CT and back recombination.

It was observed that this interfacial oxide layer does not impact the charge transfer time and still CT signal rise can be observed for TiO_2/pSi(HF), 400HT (Figure S8) and TiO_2/pSi(HF), 550HT. However, the interfacial SiO_x acts as trapping or recombination pathway for

Table 2
Characteristic charge transfer time, τ_{CT}, from pSi to TiO_2 and the carriers decay time, t_{decay}, when carrier have reached to TiO_2 and start to recombine at SiO_x interface. Excitation density used for the measurements is 200 μ J cm^{-2} at 500 nm excitation wavelength.

Samples	τ_{CT}, ps	t_{decay}
TiO_2/pSi(nat. ox.), as-dep.	600	>10 ns
TiO_2/pSi(HF), as-dep.	200	>10 ns
TiO_2/pSi(nat. ox.), 300HT	420	>10 ns
TiO_2/pSi(HF), 300HT	370	>10 ns
TiO_2/pSi(HF), 400HT	370	~8 ns
TiO_2/pSi(nat. ox.), 550HT	370	~1 ns
TiO_2/pSi(HF), 550HT	370	~5 ns

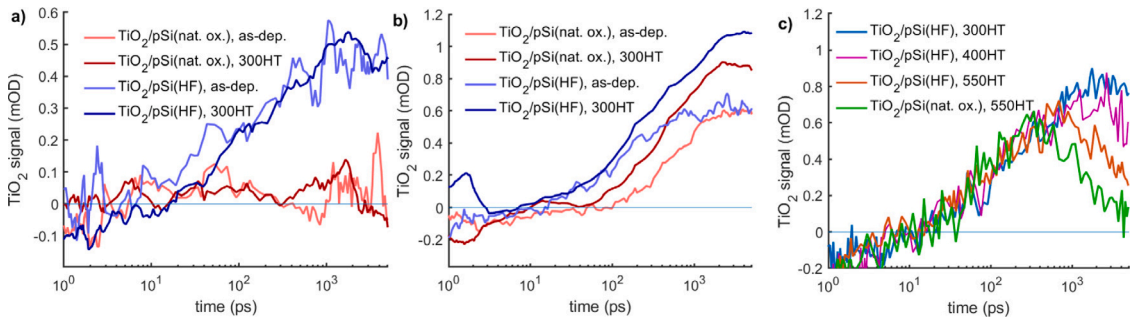

Fig. 7. TiO_2/pSi CT signal rise (decay dynamics) with 500 nm excitation probed at 700 nm for (a) low pump fluence of 24 μ J cm^{-2}, and (b) high pump fluence of 200 μ J cm^{-2}, (c) decay profiles after 500 nm excitation of different TiO_2/pSi samples probed at 700 nm, showing increased carrier losses in TiO_2 when the heat-treatment temperature is increased from 300 °C to 550 °C. Data for figure (a) and (b) were smoothed for clarity.

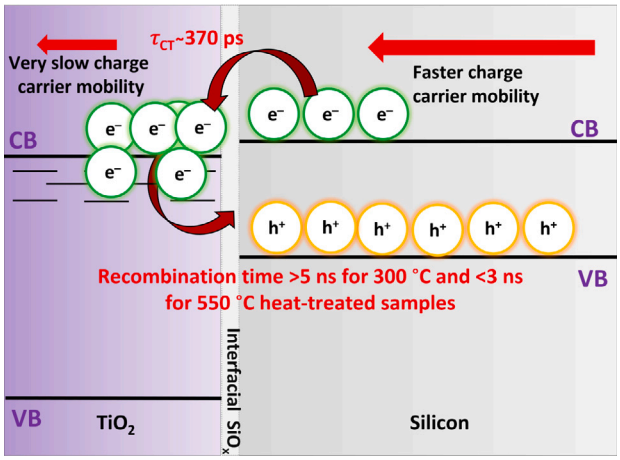

Fig. 8. Photoinduced interfacial charge transfer in TiO_2/pSi samples.

electrons from the TiO_2 back to pSi. This is shown in Fig. 7c where the decay profiles for 300–550 °C are compared at 700 nm probe wavelength for TiO_2/pSi(HF) samples excited at 500 nm. The decay profiles of 550 °C heat-treated samples show lifetimes of 5 ns and 1 ns for HF and nat. ox. samples, respectively, whereas 300 °C heat-treated samples have lifetime greater than 10 ns. This explains the sudden decrease in photocurrent when samples were heat-treated at 550 °C in the recent study by Saari et al. [24]. It is also noteworthy to find out that TiO_2/pSi(nat. ox.), 550HT sample shows similar CT rate but the recombination is more pronounced in this case. For the 300HT samples the recombination could not be distinguished in the 5 ns time range, but the 550HT results indicate that HF treated samples probably have slower back recombination than native oxide samples and therefore better device performance across all heat-treatment temperatures.

5.6. Effective minority carrier lifetime and electrical surface passivation provided by the TiO_2 thin films

PEC devices are minority carrier devices i.e., minority carriers set the limit for the output current. Therefore, it is also important to characterize the minority carrier lifetime. The minority carriers can recombine with majority carriers both inside the silicon bulk and also at the interfaces/surfaces. Since our bulk is of high quality (note that degenerated substrates are omitted from the minority carrier lifetime study), here the measured lifetime directly reflects the minority carrier recombination at the TiO_2/Si interface. From the samples fabricated on n-type Si, we obtained laterally homogeneous μ-PCD maps with an effective minority carrier lifetime of ≈ 12 μs, regardless of HF treatment and heat-treatment at 300 °C. This corresponds to an interface recombination velocity of 2700 cm s^{-1}, which can be considered relatively high. Another indicator for rather poor electrical surface passivation was the fact that the lifetime was measured to be at the same level also in the reference sample without TiO_2. As Baochen et al. [48] and Matsui et al. [49] have earlier achieved effective lifetimes in the range of several ms with ALD TiO_2surface passivation, one focus in future experiments could be to try to improve the electrical surface passivation capability without compromising the carrier transfer properties.

6. Conclusions

Since the rate and efficiency of electron transfer from silicon to TiO_2 is ambiguous, therefore, in this article, the TiO_2/Si photoelectrodes were prepared by ALD and transient reflectance spectroscopy was employed for the in-depth analysis of charge transfer dynamics at the TiO_2/Si interface. The effects of Si pre-treatment with hydrofluoric acid and post-deposition heat-treatments on the charge transfer rate from Si to TiO_2 were compared. By modelling the TR signals of Si and TiO_2, the charge transfer signals from TiO_2 and Si were differentiated and the analysis revealed that most of the charge transfer from Si to TiO_2 takes place within hundreds of picoseconds for all the samples. Growth of ALD TiO_2 on HF pre-treated SiO_x free Si improves the electron transfer time compared to films grown on Si with native oxide. However, this charge transfer time difference decreases when the samples are heat-treated at >300 °C. Increasing the HT temperature from 300 °C to 550 °C does not affect the electron transfer time (370 ps) from Si to TiO_2 but leads to reduced carrier lifetime in TiO_2 due to back recombination by the interfacial SiO_x that is detrimental to TiO_2/Si device performance in PEC applications. Also, from the pump-probe measurements, we found out that another bottleneck is the low diffusion coefficient, i.e., mobility of electrons in TiO_2 which also limits the charge transfer by their accumulation in the CB of TiO_2. By modelling the TiO_2 charge transfer signal, it can be shown that the transferred carriers go to the TiO_2/Si interface and do not travel to the surface of TiO_2. This stacking of charge carriers within the interface fills the possible energy states and eventually causes the charge transfer to stagnate and thus stop, as the carriers are unable to diffuse deeper into bulk TiO_2. Hence, the percentage of transferred carriers after 500 nm excitation drops from 24% to 4.3% when pump fluence was increased from 24 to 456 μ J cm^{-2}, respectively. However, this should not be a problem for regular devices since sunlight has much lower photon fluence in the relevant time scale of 5 ns than this pump fluence, but it could become an issue for concentrated solar devices. It should be noted that our measurement timescale does not reveal when the over-saturation bottleneck eases. Overall, by our newly developed method, ultrafast charge transfer in TiO_2/Si system is proved, but for practical devices, removal of the native oxide layer of silicon is beneficial to the charge transfer. Although the heat-treatment at ≥300 °C enhances the crystallinity in TiO_2, it also thickens the interfacial Si oxide layer. However, it appears that SiO_x does not impact the charge transfer process itself but the lifetime of carriers in TiO_2 is reduced to <3 ns for

550 °C HT samples due to the enhanced recombination at the interface. Likewise, our new TR methodology and modelling enables similar studies to be carried out for any multilayer device where traditional inorganic semiconductors are combined with any other materials or layers, such as perovskite-Si or GaAs multijunction solar cells which are of very keen interest at the moment. Although we only tested TiO_2on Si, our findings share important revelations and phenomena that one may encounter when carrying out such studies in other contexts and samples.

CRediT authorship contribution statement

Ramsha Khan: Conceptualization of this study, Investigation, Writing – original draft. **Hannu P. Pasanen:** Conceptualization of this study, Modelling of the data, Writing – draft. **Harri Ali-Löytty:** Synthesis, Review & editing. **Hussein M. Ayedh:** Investigation. **Jesse Saari:** Sample preparation. **Ville Vähänissi:** Writing – draft, Review & editing. **Mika Valden:** Validation. **Hele Savin:** Validation, Review & editing. **Nikolai V. Tkachenko:** Conceptualization of this study, Review & editing, Project administration.

Declaration of competing interest

The authors declare that they have no known competing financial interests or personal relationships that could have appeared to influence the work reported in this paper.

Data availability

Data will be made available on request.

Acknowledgements

R.K. thanks Tampere University doctoral school, Finland and Kaute foundation, Finland for the funding. J.S. was supported by the Vilho, Yrjö and Kalle Väisälä Foundation of the Finnish Academy of Science and Letters. The authors acknowledge the financial support of the Academy of Finland both via the Flagship on Photonics Research and Innovation “PREIN” and via the project numbers 320164 (H. P. P., H. A.), and 331313 (V. V.). This work was supported by the Jane & Aatos Erkko Foundation, Finland (Project ‘Solar Fuels Synthesis’). The authors acknowledge the provision of facilities and technical support by Micronova Nanofabrication Centre in Espoo, Finland within the OtaNano research infrastructure at Aalto University.

Appendix A. Supplementary data

Supplementary material related to this article can be found online at https://doi.org/10.1016/j.surfin.2023.102871.

References

[1] S. Chen, L.-W. Wang, Thermodynamic oxidation and reduction potentials of photocatalytic semiconductors in aqueous solution, Chem. Mater. 24 (2012) 3659–3666.
[2] R. Fan, Z. Mi, M. Shen, Silicon based photoelectrodes for photoelectrochemical water splitting, Opt. Express 27 (4) (2019) A51–A80.
[3] K. Sun, S. Shen, Y. Liang, P.E. Burrows, S.S. Mao, D. Wang, Enabling silicon for solar-fuel production, Chem. Rev. 114 (17) (2014) 8662–8719.
[4] H.J. Fu, I.A. Moreno-Hernandez, P. Buabthong, K.M. Papadantonakis, B.S. Brunschwig, N.S. Lewis, Enhanced stability of silicon for photoelectrochemical water oxidation through self-healing enabled by an alkaline protective electrolyte, Energy Environ. Sci. 13 (11) (2020) 4132–4141.
[5] J. Feng, M. Gong, M.J. Kenney, J.Z. Wu, B. Zhang, Y. Li, H. Dai, Nickel-coated silicon photocathode for water splitting in alkaline electrolytes, Nano Res. 8 (5) (2015) 1577–1583.
[6] Z. Xia, X. Zhou, J. Li, Y. Qu, Protection strategy for improved catalytic stability of silicon photoanodes for water oxidation, Sci. Bull. 60 (16) (2015) 1395–1402.
[7] D. Bae, B. Seger, P.C.K. Vesborg, O. Hansen, I. Chorkendorff, Strategies for stable water splitting via protected photoelectrodes, Chem. Soc. Rev. 46 (7) (2017) 1933–1954.
[8] M.J. Choi, J.-Y. Jung, M.-J. Park, J.-W. Song, J.-H. Lee, J.H. Bang, Long-term durable silicon photocathode protected by a thin Al_2O_3/SiO_x layer for photoelectrochemical hydrogen evolution, J. Mater. Chem. A 2 (9) (2014) 2928–2933.
[9] S. Hu, N.S. Lewis, J.W. Ager, J. Yang, J.R. McKone, N.C. Strandwitz, Thin-film materials for the protection of semiconducting photoelectrodes in solar-fuel generators, J. Phys. Chem. C 119 (43) (2015) 24201–24228.
[10] Y. He, T. Hamann, D. Wang, Thin film photoelectrodes for solar water splitting, Chem. Soc. Rev. 48 (7) (2019) 2182–2215.
[11] K. Oh, C. Mériadec, B. Lassalle-Kaiser, V. Dorcet, B. Fabre, S. Ababou-Girard, L. Joanny, F. Gouttefangeas, G. Loget, Elucidating the performance and unexpected stability of partially coated water-splitting silicon photoanodes, Energy Environ. Sci. 11 (9) (2018) 2590–2599.
[12] P.A. Kohl, S.N. Frank, A.J. Bard, Semiconductor electrodes: XI . Behavior of n- and p-type single crystal semconductors covered with thin films, J. Electrochem. Soc. 124 (2) (1977) 225–229.
[13] R. Khan, S. Javed, M. Islam, Hierarchical nanostructures of titanium dioxide: Synthesis and applications, IntechOpen (2018) 978–1–78923–327–8.
[14] J. Albero, Y. Peng, H. García, Photocatalytic CO_2 reduction to C2+ products, ACS Catal. 10 (10) (2020) 5734–5749.
[15] C. Cheng, W.-H. Fang, R. Long, O.V. Prezhdo, Water splitting with a single-atom Cu/TiO_2 photocatalyst: Atomistic origin of high efficiency and proposed enhancement by spin selection, JACS Au 1 (5) (2021) 550–559.
[16] A. Gautam, A. Kshirsagar, R. Biswas, S. Banerjee, P.K. Khanna, Photodegradation of organic dyes based on anatase and rutile TiO_2 nanoparticles, RSC Adv. 6 (4) (2016) 2746–2759.
[17] K. Al-Attafi, A. Nattestad, Q. Wu, Y. Ide, Y. Yamauchi, S.X. Dou, J.H. Kim, The effect of amorphous TiO_2 in P25 on dye-sensitized solar cell performance, Chem. Commun. 54 (4) (2018) 381–384.
[18] H. Hu, B. Dong, H. Hu, F. Chen, M. Kong, Q. Zhang, T. Luo, L. Zhao, Z. Guo, J. Li, Z. Xu, S. Wang, D. Eder, L. Wan, Atomic layer deposition of TiO_2 for a high-efficiency hole-blocking layer in hole-conductor-free perovskite solar cells processed in ambient air, ACS Appl. Mater. Interfaces 8 (28) (2016) 17999–18007.
[19] H. Ali-Löytty, M. Hannula, J. Saari, L. Palmolahti, B.D. Bhuskute, R. Ulkuniemi, T. Nyyssönen, K. Lahtonen, M. Valden, Diversity of TiO_2: Controlling the molecular and electronic structure of atomic-layer-deposited black TiO_2, ACS Appl. Mater. Interfaces 11 (3) (2019) 2758–2762.
[20] S. McDonnell, R.C. Longo, O. Seitz, J.B. Ballard, G. Mordi, D. Dick, J.H.G. Owen, J.N. Randall, J. Kim, Y.J. Chabal, K. Cho, R.M. Wallace, Controlling the atomic layer deposition of titanium dioxide on silicon: Dependence on surface termination, J. Phys. Chem. C 117 (39) (2013) 20250–20259.
[21] T. Rajaraman, S.P. Parikh, V.G. Gandhi, Black TiO_2: A review of its properties and conflicting trends, J. Chem. Eng. 389 (2020) 123918.
[22] R. Khan, H. Ali-Löytty, J. Saari, M. Valden, A. Tukiainen, K. Lahtonen, N.V. Tkachenko, Optimization of photogenerated charge carrier lifetimes in ALD grown TiO_2 for photonic applications, Nanomaterials 10 (8) (2020) 1567.
[23] J. Saari, H. Ali-Löytty, K. Lahtonen, M. Hannula, L. Palmolahti, A. Tukiainen, M. Valden, Low-temperature route to direct amorphous to rutile crystallization of TiO_2 thin films grown by atomic layer deposition, J. Phys. Chem. C 126 (36) (2013) 15357–15366.
[24] J. Saari, H. Ali-Löytty, M. Honkanen, A. Tukiainen, K. Lahtonen, M. Valden, Interface engineering of TiO_2 photoelectrode coatings grown by atomic layer deposition on silicon, ACS Omega 6 (41) (2021) 27501–27509.
[25] S. Fengler, H. Kriegel, M. Schieda, H. Gutzmann, T. Klassen, M. Wollgarten, T. Dittrich, Charge transfer in c-Si(n++)/TiO_2(ALD) at the amorphous/anatase transition: A transient surface photovoltage spectroscopy study, ACS Appl. Mater. Interfaces 12 (2) (2020) 3140–3149.
[26] C. Ros, T. Andreu, M.D. Hernández-Alonso, G. Penelas-Pérez, J. Arbiol, J.R. Morante, Charge transfer characterization of ALD-grown TiO_2 protective layers in silicon photocathodes, ACS Appl. Mater. Interfaces 9 (21) (2017) 17932–17941.
[27] M. Perego, G. Seguini, G. Scarel, M. Fanciulli, F. Wallrapp, Energy band alignment at TiO_2/Si interface with various interlayers, J. Appl. Phys. 103 (4) (2008) 043509.
[28] L. Santinacci, M.W. Diouf, M.K.S. Barr, B. Fabre, L. Joanny, F. Gouttefangeas, G. Loget, Protected light-trapping silicon by a simple structuring process for sunlight-assisted water splitting, ACS Appl. Mater. Interfaces 8 (37) (2016) 24810–24818.
[29] D. Wrana, T. Gensch, B.R. Jany, K. Cieślik, C. Rodenbücher, G. Cempura, A. Kruk, F. Krok, Photoluminescence imaging of defects in TiO_2: The influence of grain boundaries and doping on charge carrier dynamics, Appl. Surf. Sci. 569 (2021) 150909.
[30] S.K. Wallace, K.P. McKenna, Grain boundary controlled electron mobility in polycrystalline titanium dioxide, Adv. Mater. Interfaces 1 (5) (2014) 1400078.
[31] J.D. Park, B.H. Son, J.K. Park, S.Y. Kim, J.-Y. Park, S. Lee, Y.H. Ahn, Diffusion length in nanoporous TiO_2 films under above-band-gap illumination, Sci. Bull. 4 (6) (2014) 067106.

[32] G. Man, J. Schwartz, J.C. Sturm, A. Kahn, Electronically passivated hole-blocking titanium dioxide/silicon heterojunction for hybrid silicon photovoltaics, Adv. Mater. Interfaces 3 (15) (2016) 1600026.
[33] Y. Liu, B. Sang, M.A. Hossain, K. Gao, H. Cheng, X. Song, S. Zhong, L. Shi, W. Shen, B. Hoex, Z. Huang, A novel passivating electron contact for high-performance silicon solar cells by ALD Al-doped TiO_2, Sol. Energy 228 (2021) 531–539.
[34] H. Shen, Y. Yin, Y. Li, D. Hiller, D.A. Jacobs, H.T. Nguyen, P. Phang, G.G. Andersson, U. Kaiser, T.P. White, K. Weber, K.R. Catchpole, Efficient passivation and low resistivity for p+-Si/TiO_2 contact by atomic layer deposition, ACS Appl. Energy Mater. 3 (7) (2020) 6291–6301.
[35] H.P. Pasanen, P. Vivo, L. Canil, H. Hempel, T. Unold, A. Abate, N.V. Tkachenko, Monitoring charge carrier diffusion across a perovskite film with transient absorption spectroscopy, J. Phys. Chem. Lett. 11 (2020) 445–450.
[36] M. Wilson, J. Lagowski, L. Jastrzebski, A. Savtchouk, V. Faifer, COCOS (corona oxide characterization of semiconductor) non-contact metrology for gate dielectrics, AIP Conf. Proc. 550 (1) (2001) 220–225.
[37] R. Khan, H. Ali-Löytty, A. Tukiainen, N.V. Tkachenko, Comparison of the heat-treatment effect on carrier dynamics in TiO_2 thin films deposited by different methods, Phys. Chem. Chem. Phys. 23 (2021) 17672–17682.
[38] J. Saari, H. Ali-Löytty, M.M. Kauppinen, M. Hannula, R. Khan, K. Lahtonen, L. Palmolahti, A. Tukiainen, H. Grönbeck, N.V. Tkachenko, M. Valden, Tunable Ti^{3+}-mediated charge carrier dynamics of atomic layer deposition-grown amorphous TiO_2, J. Phys. Chem. C 126 (9) (2022) 4542–4554.
[39] L. Palmolahti, H. Ali-Löytty, M. Hannula, J. Saari, W. Wang, A. Tukiainen, K. Lahtonen, M. Valden, Pinhole-resistant nanocrystalline rutile TiO_2 photoelectrode coatings, Acta Mater. 239 (2022) 118257.
[40] T. Niewelt, B. Steinhauser, A. Richter, B. Veith-Wolf, A. Fell, B. Hammann, N. Grant, L. Black, J. Tan, A. Youssef, J. Murphy, J. Schmidt, M. Schubert, S. Glunz, Reassessment of the intrinsic bulk recombination in crystalline silicon, Sol. Energy Mater. Sol. Cells 235 (2022) 111467.
[41] H.P. Pasanen, P. Vivo, L. Canil, A. Abate, N. Tkachenko, Refractive index change dominates the transient absorption response of metal halide perovskite thin films in the near infrared, Phys. Chem. Chem. Phys. 21 (27) (2019) 14663–14670.
[42] D.E. Aspnes, A.A. Studna, Dielectric functions and optical parameters of Si, Ge, GaP, GaAs, GaSb, InP, InAs, and InSb from 1.5 to 6.0 eV, Phys. Rev. B 27 (1983) 985–1009.
[43] J.R. DeVore, Refractive indices of rutile and sphalerite, J. Opt. Soc. Amer. 41 (6) (1951) 416–419.
[44] M.A. Green, M.J. Keevers, Optical properties of intrinsic silicon at 300 K, Prog. Photovolt. 3 (1995) 189–192.
[45] H. Zaghloul, M. Emam, M. Abdelrahman, M. Abd Rabbo, Optimization and parametric analysis of a multi-junction high-concentrator PV cell combined with a straight fins heat sink, Energy Convers. Manag. 243 (2021) 114382.
[46] G. Zubi, J.L. Bernal-Agustín, G.V. Fracastoro, High concentration photovoltaic systems applying III–V cells, Renew. Sustain. Energy Rev. 13 (9) (2009) 2645–2652.
[47] B. Gallas, A. Brunet-Bruneau, S. Fisson, G. Vuye, J. Rivory, SiO_2–TiO_2 Interfaces studied by ellipsometry and X-ray photoemission spectroscopy, J. Appl. Phys. 92 (4) (2002) 1922–1928.
[48] B. Liao, B. Hoex, A.G. Aberle, D. Chi, C.S. Bhatia, Excellent c-si surface passivation by low-temperature atomic layer deposited titanium oxide, Appl. Phys. Lett. 104 (25) (2014) 253903.
[49] T. Matsui, M. Bivour, P.F. Ndione, R.S. Bonilla, M. Hermle, Origin of the tunable carrier selectivity of atomic-layer-deposited TiOx nanolayers in crystalline silicon solar cells, Sol. Energy Mater. Sol. Cells 209 (2020) 110461.